VOL. 18, NO. 11, JUNE 2023 ISSN 1819-6608
ARPN Journal of Engineering and Applied Sciences

www.arpnjournals.com

MODELLING THE SPATIAL-TEMPORAL EXPANSION OF LASER-PRODUCED TIN (SN) PLASMA WITH FEMTOSECOND LASER

Huda Oda Saheb and Wissam H. Mahdi wisam
Department of Physics, Faculty of Education for Girls, University of Kufa, Najaf, Iraq
E-Mail: hudaoda2020@gmail.com

ABSTRACT

In this study, the 1-D hydrodynamic code (MED103) has been used to simulate the Tin (Sn) plasma in space and time with 400 cells as mesh and 10 ns simulation time that is produced by laser with the pulse of 500 fs and its wavelength of 1064 nm. Unique radiation sources of extreme ultraviolet and soft X-ray emissions can be generated from the high ions of laser-produced heavy element plasmas. The spatial-temporal distribution of Sn plasma parameters was studied when a laser pulse was focused on a target to 100 µm diameter with the intensity of $1.27 * 10^{15}$ w/cm^2. There are two peaks of pressure, first inside the target after laser pulse time and the other close to the surface of the target at a time of 8 ns which is higher than 30 ≈ Mbar. The pressure is still high during simulation time. During and after the laser pulse time, the electron and ion temperature reaches maximum value but their values are not equal.

Keywords: tin plasma, femtosecond laser, EUV emissions, med103 code.

Manuscript Received 17 February 2023; Revised 24 July 2023; Published 13 August 2023

1. INTRODUCTION

Future generations of computer processors as well as other integrated circuits, which have been in development for decades, will be powered by this technological advancement. Since it has taken a while to develop such a complex technology into mass production, interest in light sources near 6.7 nm has recently grown to create the lithography of the next generation., called "extreme ultraviolet lithography"[1]

Laser plasma EUV light sources play a vital role in the fields of microscopic imaging, material analysis, and EUV lithography. In particular, extreme ultraviolet lithography technology is the key technology required to manufacture integrated circuits with nodes below 7 nm, and it is also a shortboard in my country's high-end chip research and development. In the extreme ultraviolet lithography technology, the extreme ultraviolet light source needs to use its matching optical components. [2, 3]. As a result, the lithography light source needed to realize chips with smaller node sizes has a wavelength of 13.5 nm in the extreme ultraviolet range. In recent years, researchers have begun to study the 13.5 nm (2% bandwidth) in-band extreme ultraviolet light radiation characteristics and conversion efficiency have been studied a lot. Compared with other targets, the extreme ultraviolet light source generated by Sn target plasma has higher conversion efficiency, and it can produce a high cleanness and broadband spectrum in the 13.5 nm (2% bandwidth) band [4]. The above characteristics make the Sn target 13.5 nm extreme ultraviolet light source a required light source in the extreme ultraviolet lithography system, and the research on the radiation characteristics of the Sn target 13.5 nm light source has a certain research value so that it can be used in metrology and extreme ultraviolet lithography masks. There are also important applications in detection and other fields.[5, 6]

To obtain a higher conversion efficiency to meet the requirements of the lithography system, researchers have realized the laser wavelength, pulse width, target density, and double pulse by changing the laser wavelength. High conversion efficiency. In addition, the researchers found that the structural target affects the intensity of EUV radiation and the conversion efficiency [7].

2. THEORY

The ponderomotive force of an ultrashort and ultra-intense laser generates a longitudinal accelerating electric field in laser-plasma electron accelerators. Plasma electrons are pushed to come out of the laser beam's trajectory by this force, which is proportional to the laser intensity gradient, which is splatted from the ions[8]. This results in a traveling electric field that propagates linearly This is ideal for giving the particles a proportional acceleration of their energy and has a phase velocity that is close to the speed of light in the wake of the laser beam. An electric field (E) has an amplitude of hundred Gigavolts for each per meter. Furthermore, the plasma wavelength is the Distinctive scale of the length field, 10-30 µm for electron densities ne = 1018-1019 cm^3. The amount of plasma generated varies depending on the target material, focusing conditions, laser intensity, pulse duration, and wavelength. The plasma is produced at a low level of density, in a high-level temperature in contrast to the caused reverse shock by the atomizing pressure, falling towards the target surface The material is left to the target behind the front of the fall at a finite temperature and a super density compared to the initial density of the material.[9, 10].

In this research, a theoretical simulation was performed using an updated version of the MED103 (Medusa) hydrodynamic code. The study of the spatial and temporal evolution (STV) of some LPP (Gd) properties,

such as ion mass density ni, (P) pressure, and (V) velocity, was conducted to understand plasma conditions. [11]

The interaction's timescale, which ranges from a femtosecond to nanoseconds, is highly influenced by how long the incident laser pulse lasts [12]. where the formation of laser-produced plasmas is a rapid process that has been under research for several decades due to its versatile and complex nature. When a laser pulse of high energy density is struck at the surface of a target for a very short period, it instantly excites, ionizes, and vaporizes the electrons into a superheated column of vapor, also called a "plasma column"

The process's absorption coefficient, K, can be written as [13]:

$$k = 2^5, e^4 \left(\frac{2c^2\pi}{k_b m_e}\right)^{\frac{3}{2}} and \frac{n_{ec}}{w_l} z^2 \ln(\Lambda) \frac{1^{e^4}}{(w_l^2 - w_p^2)^{0.5}} \quad \ldots\ldots (3)$$

Where:

e: charge of the electron, c speed of light in vacuum, kB is Boltzmann constant, m: mass of the electron, nec (critical electron number density for the laser pulse), Z: Ionization degree, wp: plasma frequency. [14]

3. RESULTS AND DISCUSSIONS

The program MED103 used code 1-D hydrodynamic to simulate Laser produced (Sn=50) plasmas (a developed version of Medusa) [15]. The program MED103 used code 1-D hydrodynamic to simulate plasmas of Laser produced from the (Sn=50) (a developed version of Medusa), the pulse laser wavelength (λ =1064 nm), (ρ) it's the density of power ($1*10^{15}$ w.cm^{-2}) and (FWHM) width of pulse = 500 fs, fall on the Target with Cylindrical geometric radius shape (100 µm). The simulation time for the entire process was set to (10 ns) and the default mesh size for the cylindrical target was 400 cells with a time-step of (500 fs).

3.1 Pressure Distribution in Space and Time

In the first Figure-1 (A, B, C) the pressure begins near the target surface at (10^2 $Mbar$), then gradually decreases to (10^{-4} $Mbar$) at a (220 µm) distance. The time variation also has a similar behavior, as shown in Figure B, the pressure value reaches (10^{-4} $Mbar$) at the edge of the plasma at a (10 µm) distance. We notice the pressure decreases with increasing the distance from the edge of the metal surface, after the end of the laser pulse, the pressure will decrease gradually due to the decrease in the density and the velocity of the plasma expansion.

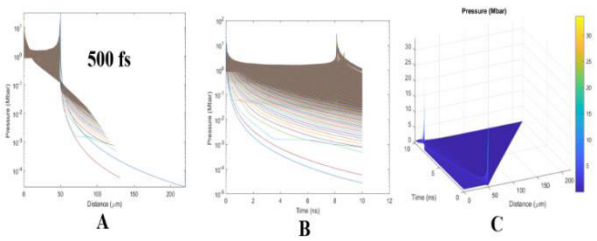

Figure-1. Sn plasma pressure as a function of distance and time, (A) PPV in space, (B) PPV in time, (C) PPV in space and time.

Table-1. The maximum value of plasma pressure (in both space and time) was obtained from MED103 software simulations of tin plasma.

Pulse duration (fs)	Maximum value: p (Mbar)	Time ns	Distance µm
500	33.695	8.12383	49.871

3.2 Te Variation in Space and Time

Figure-2 (a, b) depicts the development of the Electron Temperature of Sn when plasma is created using a laser with a 500 fs pulse (FWHM) and demonstrates the importance of the electron temperature as a plasma parameter. Te of first plasma created reaches an energy value of above of 135.42 eV at a distance of 50 µm. on the surface of the tin metal target. Then the temperature of the electrons begins to decrease until it reaches about 10 eV.

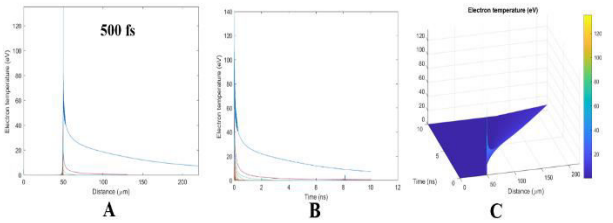

Figure-2. The Sn plasma in space and time evolution of electron temperature, (A) variation in space, (B) variation in time, (C) variation in space and time.

Table-2. The maximum value of the electrons temperature (in time and space) resulting from the MED103 program simulation of tin plasma.

Pulse duration (fs)	Maximum value: Electron Temperature(ev)	Time ns	Distance µm
500	135.42	0.00673171	49.842

3.3 Ti Variation in Space and Time

Figure-3 (A, B) illustrate the temperature of the ions with distance and time at a laser pulse duration of 500 fs. We notice the evolution of the plasma with a 50 µm distance of an Sn surface face, the maximum value of the ion's temperature, Ti, reaches 70 ev, after which it reaches 10 ev at 200 µm in (10 ns).

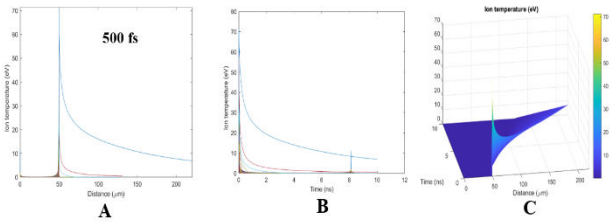

Figure-3. The evolution of ion temperature of Sn plasma in space and time, (A) variation in space, (B) variation in time, (C) variation in space and time.

Table-3. The maximum value of the temperature of ions (in time and space) resulting from the MED103 program simulation of tin plasma.

Pulse duration (fs)	Maximum value: ion T(eV)	Time ns	Distance µm
500	71.216	0.00508009	49.851

3.4 Spatial and Temporal Ion Rate Z* Variation

Figure-4 (A, B) At the beginning of the reaction, we notice the plasma resulting from a laser pulse of 500 fs duration, which develops at 50 µm from the Sn surface face target, and the maximum value of the ion rate Z* is (10.966), then it falls and stabilizes at (7.5) until the end of the laser simulation time as shown in Figure (C) indicates the three-dimensional spatial and temporal distribution of the ion rate.

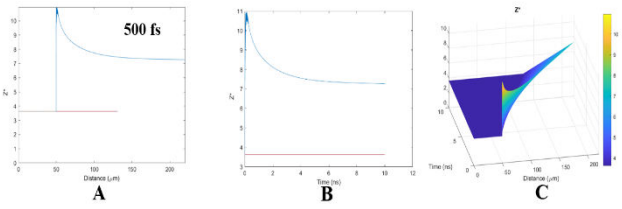

Figure-4. The evolution of ionization (Z*) of Sn plasma in space and time, (A) spatial Z* variation, (B) temporal Z* variation, (C) spatial-temporal distribution of Z*.

Table-4. The maximum value of ionic rate (in time and space) was obtained from the MED103 simulation of tin plasma.

Pulse duration (fs)	Maximum value: Z^*	Time ns	Distance µm
500	10.966	0.137965	51.065

3.5 Spatial and Temporal Velocity Variation

The velocity of the plasma increases spatially and temporally, and Plasma is formed from the outer surface in contact with the incident laser wave. For an ultra-short pulse at the target surface [16], the velocity starts from zero and then increases with plasma formation to be less than (20×10^5 cm/sec) at a distance of 50 µm. After the end of the laser pulse, the plasma expansion velocity increases to (20×10^7 cm/sec).) At a distance (220 µm). And the expansion of the plasma within 10 ns in time, taking into account that the kinetic energy of the electrons and ions will increase as a result of the high temperature of the out-face Sn, which successively gets to the velocity of expansion of the plasma as in Figure-5 (A and B), C indicates the three-dimensional spatiotemporal distribution of the electron velocity, Ve, in the plasma.

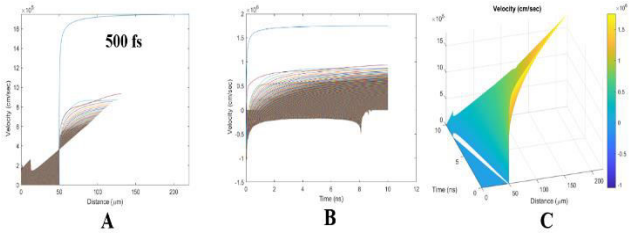

Figure-5. The spatial and temporal variation of Sn plasma velocity, (a) plasma velocity variation in space, (b) plasma velocity variation in time, (C) plasma velocity variation in space and time.

Table-5. The maximum value of electron velocity Ve (in time and space) resulting from MED103 simulation of tin plasma.

Pulse duration (fs)	Maximum value: velocity (cm/sec)	Time ns	Distance µm
500	1751000	9.92859	216.35

4. CONCLUSIONS

laser pulse duration in femtosecond at (500 fs) with laser wave intensity of $2.1\text{x}10^{15}$ w cm^{-2} and λ of 1064 nm was fired at an Sn target, we used the 1-D hydrodynamic MED103 code to study the laser plasma properties and track the evolution of a few hydrodynamic plasma parameters, the electron density was determined at the first times of the plasma created at the target of pulse duration 500 fs, the electron temperature seen reach at the top value of 140 eV during, immediately after a laser pulse, the electron density have the maximum at 1024 cm^{-3} and exhibits the constant pressure behaviour. A maximum temperature of ions, Ti, reaches 70 eV. The maximum value of the ion rate is Z *. The plasma expansion velocity increases to (20×10^7 cm/sec). At a distance (220) µm. The physical processes range in magnitude and time from the fs time scales of the laser-driven plasma processes to the fluid dynamics initiated by the laser impact that cause the deformation of the tin target. The development of the physical understanding of

the atomic plasma processes and the engineering necessary to realize high output powers, which led to the adoption of EUV nanolithography in high-volume manufacturing, is responsible for the striking improvement in industrial source performance over the past few years. Not only from gas-laser-driven systems but also from solid-state laser-driven plasma sources, more advancement is anticipated. Strong interaction and collaborations between fundamental research and industrial innovations have, are, and will continue to be the main drivers of progress in this field.

ACKNOWLEDGEMENTS

The support of the graduate laboratory of the Physics Department of Physics, Faculty of Education for Girls, University of Kufa Najaf, Iraq.

REFERENCES

[1] U. Chaulagain *et al*. 2022. ELI Gammatron Beamline: A Dawn of Ultrafast Hard X-ray Science. In Photonics. 9(11): MDPI, 853.

[2] K. Sugimoto, N. Higashi, N. Iwata, A. Sunahara, T. Sano, and Y. Sentoku. 2020. PIC simulation for dense high Z plasma formation with ultrashort petawatt laser including radiation processes. High Energy Density Physics. 36: 100816.

[3] R. Tommasini *et al*. 2017. Short pulse, high-resolution, backlighters for point projection high-energy radiography at the National Ignition Facility. Physics of Plasmas. 24(5): 053104.

[4] M. Valdivia, G. Collins IV, F. Conti and F. Beg. 2022. Wire, hybrid, and laser-cut X-pinches as Talbot–Lau backlighters for electron density diagnostics. Plasma Physics and Controlled Fusion. 64(3): 035011.

[5] H. Kiriyama *et al*. 2018. High-contrast high-intensity repetitive petawatt laser. Optics letters. 43(11): 2595-2598.

[6] A. Serafetinides and M. Makropoulou. 2019. towards bridging non-ionizing, ultra-intense, laser radiation and ionizing radiation in cancer therapy. In 20th International Conference and School on Quantum Electronics: Laser Physics and Applications, 11047: SPIE, 1104702.

[7] H. Kiriyama *et al.* 2020. Petawatt femtosecond laser pulses from titanium-doped sapphire crystal. Crystals. 10(9): 783.

[8] V. Istokskaia *et al*. 2022. Hard x-rays measurements using a scintillator-array calorimeter in high-intensity laser-plasma experiments. In Hard X-Ray, Gamma-Ray, and Neutron Detector Physics XXIV. 12241: SPIE, 117-122.

[9] A. Poyé *et al*. 2015. Dynamic model of target charging by short laser pulse interactions. Physical Review E. 92(4): 043107.

[10] A. Latif, I. Fareed, S. Siddique and M. D. Khan. 2022. Surface morphological, electrical and mechanical properties of nanosecond & femtosecond laser exposed copper, zinc and cupronickel. Nuclear Instruments and Methods in Physics Research Section B: Beam Interactions with Materials and Atoms. 517: 24-32.

[11] P. Rodgers, S. Rose and A. Rogoyski. 1989. MED101: A laser-plasma simulation code. User guide. Rutherford Appleton Lab.

[12] A. K. Mills, T. Hammond, M. H. Lam and D. J. Jones. 2012. XUV frequency combs via femtosecond enhancement cavities. Journal of Physics B: Atomic, Molecular and Optical Physics. 45(14): 142001.

[13] M. Key. 2017. Introduction to the Physics and applications of Laser Produced Plasmas. In Laser-Plasma Interactions 4: CRC Press. pp. 1-17.

[14] V. K. Meader, M. G. John, L. M. Frias Batista, S. Ahsan and K. M. Tibbetts. 2018. Radical chemistry in femtosecond laser plasma: photochemical reduction of Ag+ in liquid ammonia solution. Molecules. 23(3): 532.

[15] A. Cummings, G. O'Sullivan, P. Dunne, E. Sokell, N. Murphy and J. White. 2005. Conversion efficiency of laser-produced Sn plasma at 13.5 nm simulated with a one-dimensional hydrodynamic model and treated as a multi-component blackbody. Journal of Physics D: Applied Physics. 38(4): 604.

[16] A. Sasaki, A. Sunahara, K. Nishihawra, T. Nishikawa, F. Koike and H. Tanuma. 2008. Detailed atomic modeling of Sn plasmas for the EUV source. In Journal of Physics: Conference Series, 112(4): IOP Publishing, 042062.